

THE STAR FORMATION NEWSLETTER

No.255 - 11 March 2014

2014/4/18

izumi natsuko (D2)

16-20

“A WISE Survey of Circumstellar Disks in Taurus”

to

“High-resolution Ultraviolet Radiation Fields of Classical
T Tauri stars”

A WISE Survey of Circumstellar Disks in Taurus

T.L.Esplin et al.

- Studies of star and planet

- 星形成領域内のcircumstellar diskの検出

- それらのdiskの正確な分類

- ↑ 両方とも warm circumstellar diskからのMid infrared continuum emissionが有用

- Survey of circumstellar disks

- Data : Wide-field Infrared Survey Telescope Explore (WISE) data

- Spitzer Space telescope data

- ↑空間分解能において、WISEはSpitzerに劣るが、全天のデータを持っている。

- その他、2MASS, USNO, IRAC, MIPS等のデータも使用

- Region : Taurus star-forming region

●Conclusion

-Excess emissionを用いてTaurus内のcircumstellar diskを検出

-検出したdiskの進化段階を推定 (full, transitional, evolved, evolved transitional, debris disk)

↑ 31の新たなfull disk と16の新たなtransitional, evolved, evolved transitional, debris disk
候補を検出

-WISE All-Sky Source Catalogueを用いて新たなdisk-bearing membersの検出

↑可視や近赤外のデータも用いて、スペクトル型がM1-M7であるmemberを
新たに26天体検出

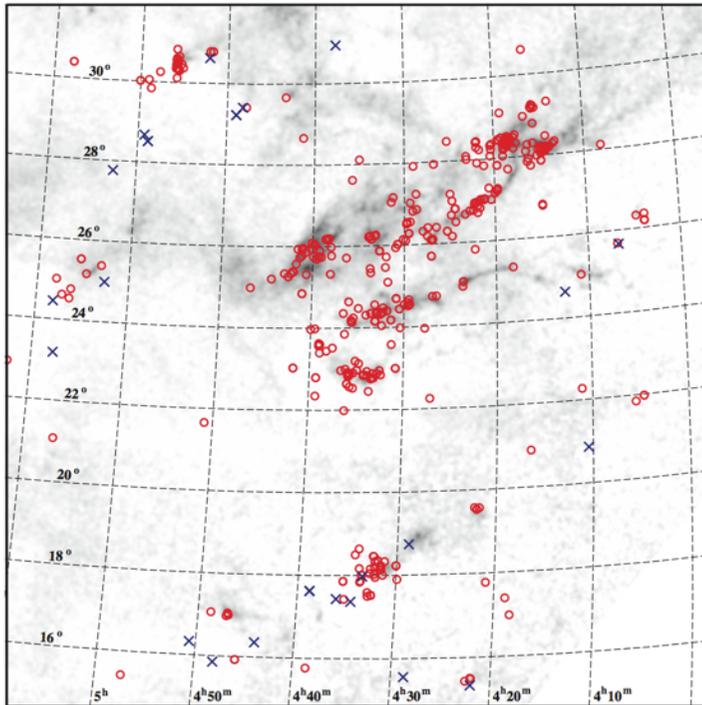


Fig. 1.— Spatial distribution of previously known members of the Taurus star-forming region (circles) and new members from this work (crosses). The dark clouds in Taurus are displayed with a map of extinction (gray scale; Dobashi et al. 2005).

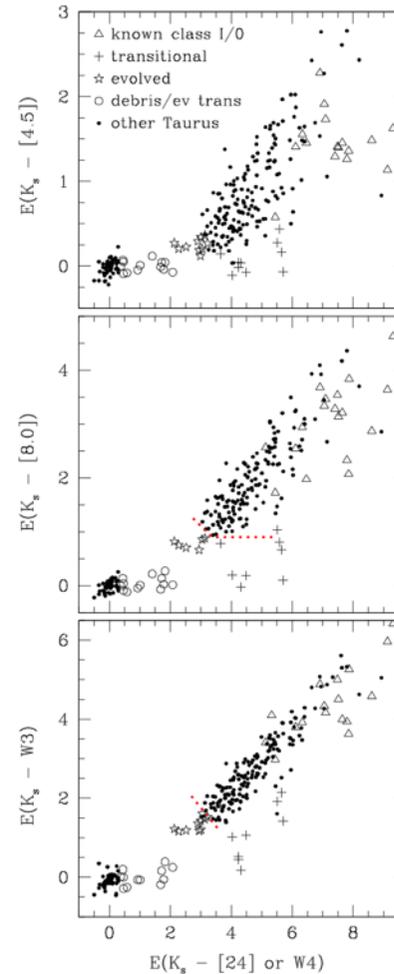


Fig. 3.— Extinction-corrected IR color excesses for members of Taurus. Data at 4.5 and 24 μm from *Spitzer* are shown when available. Otherwise, measurements at similar wavelengths from *WISE* are used (*W2* and *W4*). We have indicated known protostars (class I and 0, triangles), candidate transitional disks (crosses), candidate evolved disks (stars), and candidate debris disks or evolved transitional disks (circles). The reddest protostars are beyond the limits of these diagrams. In the middle and lower diagrams, we have marked the lower boundaries that we have adopted for full disks (dotted lines).

Thermodynamics of the dead-zone inner edge in protoplanetary disks

Julien Faure et al.

- Protoplanetary disk の inner boundary (between the turbulent and laminar region)
 - Context : 惑星が形成される領域として期待されている
界面ではthermodynamicsとturbulent dynamicsが絡み合っている
↑ただし境界の数値モデルはthermodynamicsを無視しており、物理状態をとらえきれていない
 - Aim : thermodynamicsとdiskのinner regionのdynamics (turbulent heating + dependence of the resistivity on the local temperature)の相互作用を数値的に調べる
領域はbistable regionからinner dead-zone (region of cold quiescent gas) boundaryまで (real Magnetorotational Instability (MRI) turbulenceとthermodynamicsの相互作用を理解する)
 - Method : Godunov code RAMSESを用いる
protoplanetary diskに対する3D global numerical simulations
in cylindrical limit, turbulent heatingとprescription for radiative coolingを含む
 - Conclusion: simulationはthermodynamicとturbulent dynamicsの複雑な相互作用を描写している

DNC/HNC and N^2D^+/N^2H^+ ratios in high-mass star forming cores

F.Fontani et al.

- 重水素比 DNC/HNC, N^2D^+/N^2H^+ について

- N^2D^+/N^2H^+ : pre-protostellar core → protostellar birth の段階で急激に現象

- DNC/HNC : に比べてかなり長い時間constantに存在

- ↑ Chemical model (Sakai et al. 2012)

- : observational results (Fontani et al.2011, Sakai et al 2012)を部分的に説明

- sampleが異なるため厳密な比較できない

- 同じsampleを用いて、 N^2D^+/N^2H^+ と N^2D^+/N^2H^+ を比較したい ← 本観測の目的

- 観測

- Telescope : Nobeyama 45 m telescope

- : $HN^{13}C(1-0)$, DNC (1-0) transitions

- Target : 22 high-mass core

- 8 high-mass starless cores (HMSCs), 7 high-mass protostellar objects (HMPOs)

- 7 ultracompact HII regions (UCHIIs)

- ↑ 既にIRAM 30 m telescopeを用いてに N^2D^+/N^2H^+ については観測されている。

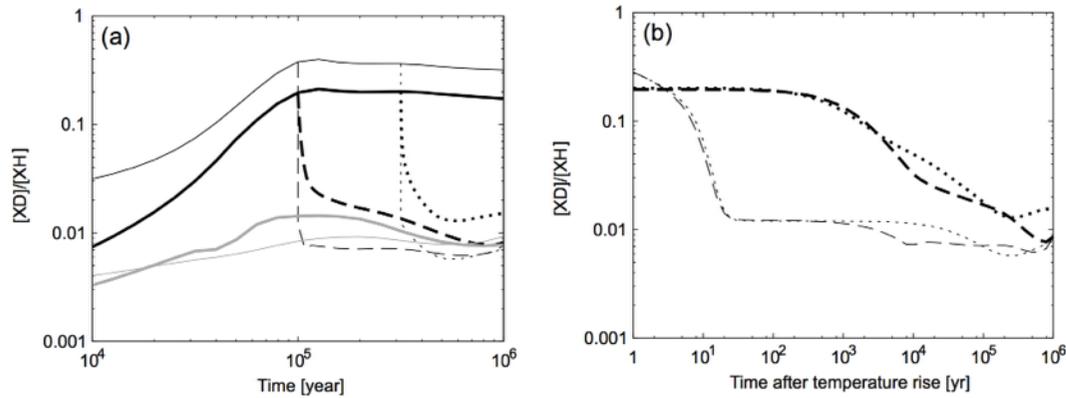


Figure 1. (a): chemical model calculation of the time dependence of DNC/HNC (thick lines) and N_2D^+/N_2H^+ (thin lines). In addition to the constant temperature cases (10 K = solid black, 30 K = solid grey), the cases in which the temperature suddenly rises from 10 to 30 K at a given age, 1×10^5 yr (dashed) or 3×10^5 yr (dotted) are shown. See Section 4.2 for the detail of the chemical model.

(b): same as panel (a), but the time starts from when the temperature increases from 10 K to 30 K.

●結果

-Sakai et al. 2012のモデルによる予測が成り立つことを確認

-重水素比は温度の上昇によるものであるが、 N_2D^+ の方がより敏感である

→DNC, N_2D^+ が似ているのに減少するタイムスケールが異なるのはこのせい

→high-mass starless coreを見つけるには N_2D^+ が適している。

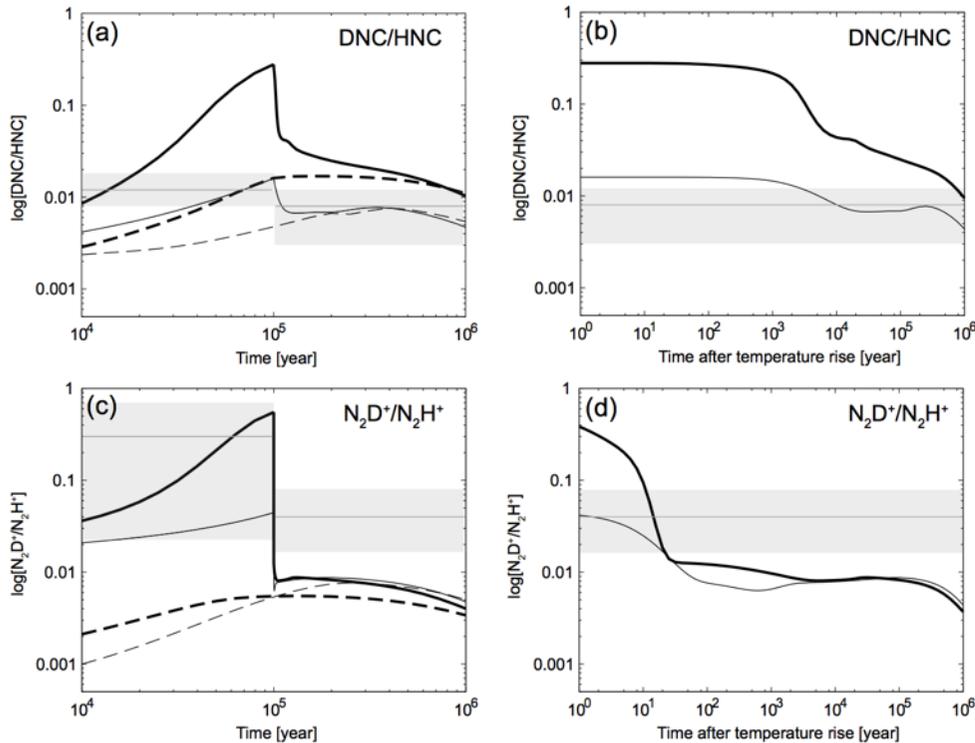


Figure 4. (a): temporal variation of the DNC/HNC abundance ratio as predicted by the chemical model described in Sect. 4.2. Solid lines represent the model with a temperature jump from 15 to 40 K at 10^5 yrs, while dashed lines represent the model with constant temperature of 40 K during 10^6 yrs. Thin and thick lines represent the model with $n_{H_2} = 10^4 \text{ cm}^{-3}$ and 10^5 cm^{-3} , respectively. The horizontal grey lines and areas indicate the average values and dispersion obtained from the observational data in this work.

(b): same as (a) for N_2D^+/N_2H^+ . The observational data here are from Fontani et al. (2011).

(c) and (d): same as (a) and (b), respectively, but the time starts from when the temperature increases from 15 K to 40 K.

Triple trouble for XZ Tau: deep imaging with the Jansky Very Large Array

D.Forgan et al.

●観測

- Telescope : The Karl G. Jansky Very Large Array (VLA)
↑ resolution - 55 milliarcsec
- Wavelength : 7 mm
- Target : XZ Tau

●XZ Tau

- XZ Tau A, XZ Tau Bからなる連星系
- 2004年のVLAによる観測により、XZ Tau AがTau A, Tau Cからなることが分かった

Carrasco-Gonzales et al. 2009

●XZ Tau A と Tau C

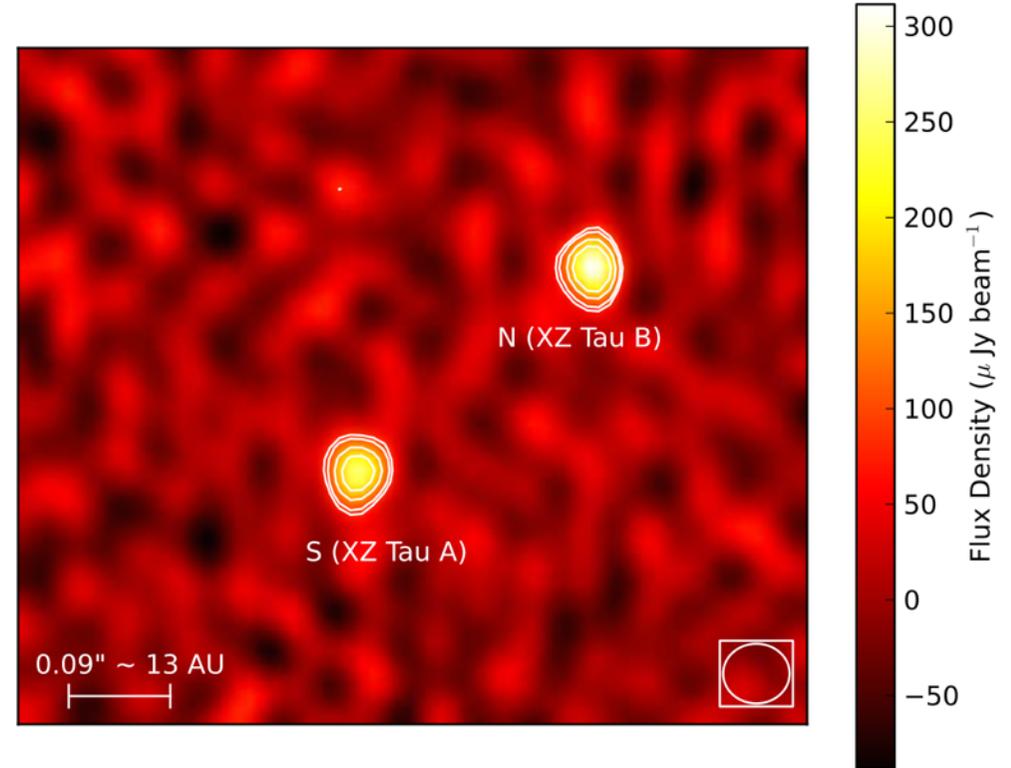
- Separation : ~13 AU
- Orbital period : ~40 Myr
- 近星点通過時にTau Aからoutflowが放出された?? (1980)

- 観測結果

- Tau C 検出されず

- Tau A, Tau Bに関してはその位置、

- 軌道等過去の研究と矛盾しない



- Tau Cが検出されない理由: 4つの仮説

- (1) Tau CはXZ Tau の系から外に出された ← 証拠ないので除外

- (2) 2004年の観測で検出されたTau Cはtransientであった ← 可能性低いが否定できない

- (3) Tau CはちょうどTau Aの前を通過している時であった

- (4) 実はTau Cは存在しない (2004の結果はミス?)

High-resolution Ultraviolet Radiation Fields of Classical T Tauri Stars

Kelvin France et al.

•Far-Ultraviolet (FUV; 912-1700Å ; Disk chemistry, Disk evolutionの情報得られる)のデータを解析

-Telescope : Hubble Space Telescope

-Wavelength : 1150 - 1700 Å (spectroscopic)

-Target : 16 Classical T Tauri Star (CTTS)
↑ Dust diskが進化段階にあるもの

-Data : high spectral resolution data + high S/N data
→ high-resolution intrinsic stellar+accretion FUV radiation fields

-FUV radiation field
: FUV continuum, reconstructed Ly α emission line, hot gas emission lines
(NV, CIV, HeII.....)

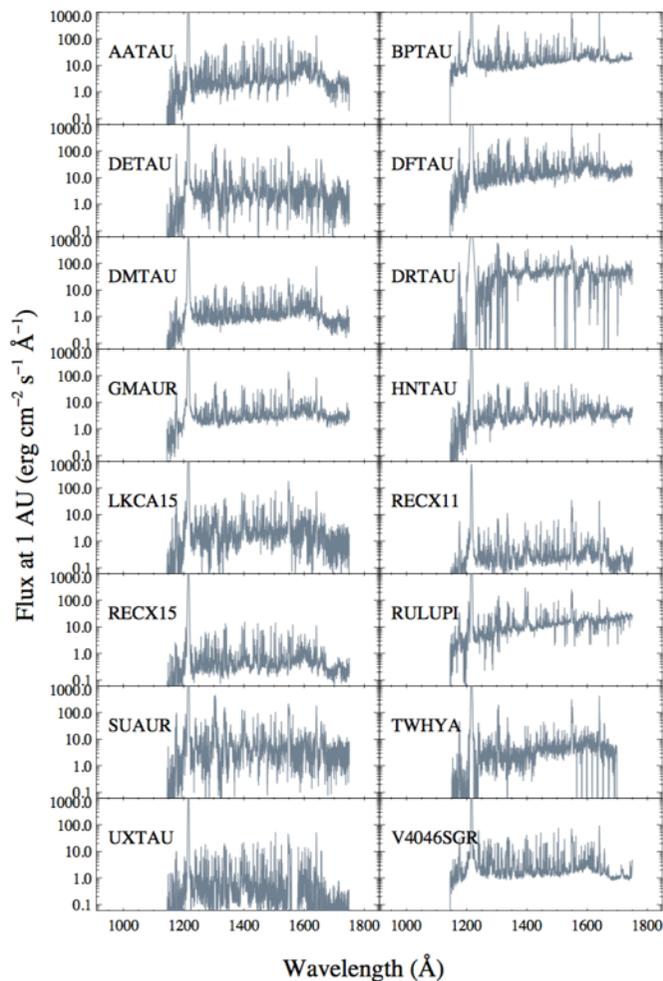


FIG. 1.— Complete FUV spectra of the 16 CTTSs studied in this work, including reconstructed Ly α emission lines. These spectra are coadditions of *HST*-COS observations in the G130M and G160M modes (except for TW Hya, which was observed with STIS E140M; Herczeg et al. 2002) at several central wavelengths and focal-plane split positions. Almost all of the structures seen in these data are real atomic and molecular emission and absorption features. The data have been corrected for interstellar reddening (Table 1), scaled to the flux at 1 AU from the central star for comparison, and binned by three spectral resolution elements (21 pixels) for display.

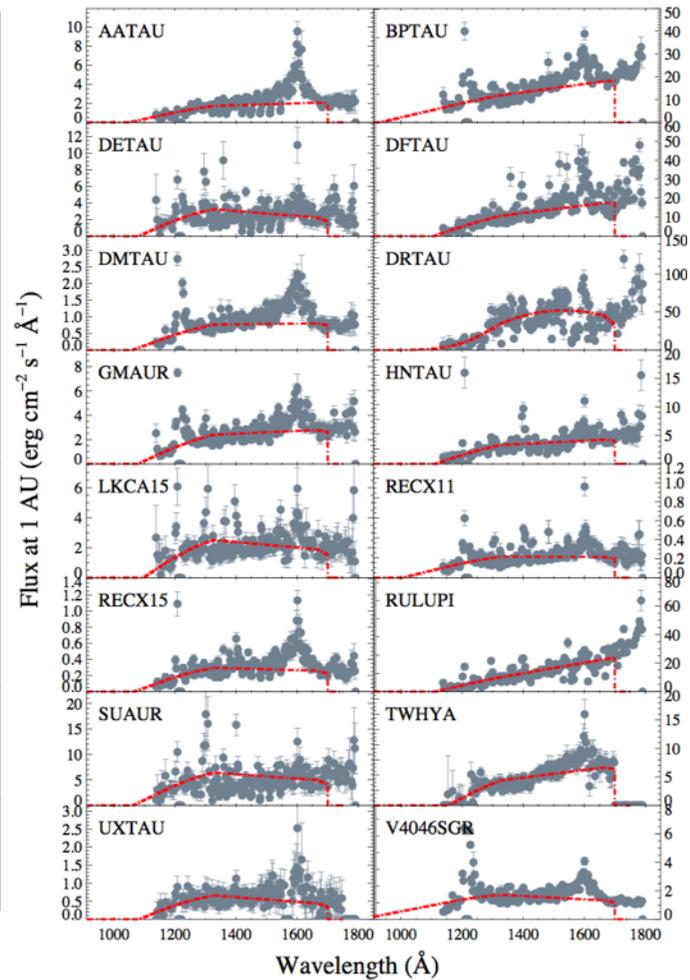


FIG. 2.— The binned FUV continuum spectra are shown as gray filled circles. A second order polynomial fit is extrapolated down to the Lyman Limit (912 Å) and is shown as the red dashed line. The “1600 Å Bump” (spanning $\sim 1520 - 1660$ Å) is prominent (detected at $> 3\sigma$ significance) in 10/16 targets.

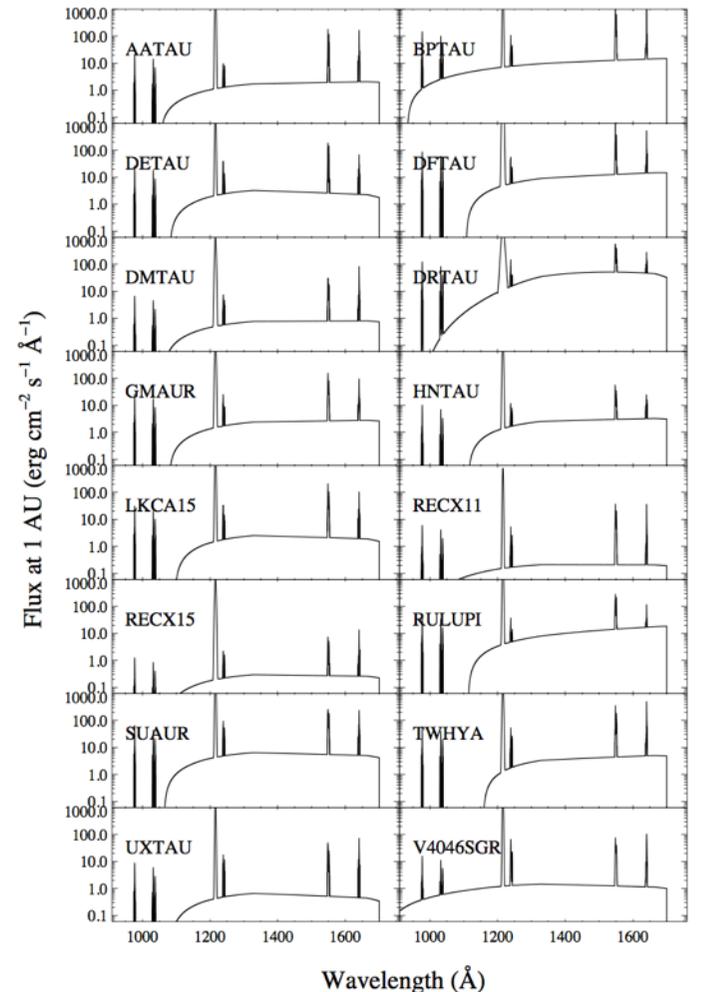


FIG. 4.— Combined intrinsic CTTS FUV radiation fields, normalized to the flux at 1 AU from the central star for comparison. These spectra include a polynomial fit to the observed FUV continuum, reconstructed Ly α radiation fields based on fluorescent H $_2$ emission lines, and observationally determined hot gas emission lines. These spectra are available in machine readable format at: http://cos.colorado.edu/~kevinf/ctts_fuvfield.html.

TABLE 2
RELATIVE CONTRIBUTIONS TO THE STELLAR + ACCRETION FUV RADIATION FIELD

Target	F_{tot}^a ($\text{erg cm}^{-2} \text{s}^{-1}$)	$\log_{10}(F_{tot}/G_o)^b$	FUV Continuum (%)	$\text{Ly}\alpha^c$ (%)	C IV (%)	Other lines ^d (%)	$\lambda \leq 1110 \text{ \AA}$ (%)
AATAU	3.1×10^4	7.3	2.8	95.9	0.8	0.6	0.1
BPTAU	3.5×10^4	7.3	16.8	75.7	4.5	3.1	1.8
DETAU	1.5×10^4	7.0	9.2	88.0	2.0	0.9	0.3
DFTAU	2.3×10^5	8.2	2.1	97.2	0.4	0.2	0.1
DMTAU	4.3×10^3	6.4	8.4	88.0	1.7	1.9	0.3
DRTAU	4.0×10^4	7.4	46.2	49.4	3.3	1.0	0.7
GMAUR	1.2×10^4	6.9	9.9	86.2	2.4	1.5	0.4
HNTAU	1.2×10^4	6.9	10.1	88.4	0.9	0.5	0.1
LKCA15	1.6×10^4	7.0	6.5	90.4	2.1	1.0	0.3
RECX11	2.3×10^3	6.2	4.6	90.9	2.9	1.7	0.6
RECX15	4.8×10^3	6.5	2.8	96.7	0.3	0.3	0.1
RULUPI	2.8×10^4	7.2	17.6	79.8	2.0	0.7	0.3
SUAUR	3.3×10^4	7.3	8.4	88.3	2.1	1.2	0.4
TWHYA	9.7×10^3	6.8	16.7	71.9	6.5	4.9	0.9
UXTAU	5.6×10^3	6.5	4.8	92.2	1.7	1.3	0.3
V4046SGR	1.5×10^4	7.0	5.3	91.8	1.2	1.8	0.9
Average ^e		7.0 ± 0.5	8.4 ± 5.2	88.1 ± 7.3	2.1 ± 1.6	1.4 ± 1.2	0.5 ± 0.4

^a Integrated 912 – 1650 Å stellar+accretion FUV radiation field (not including molecular fluorescence lines, low-ionization atomic emission, or the “1600 Å Bump”), evaluated at 1 AU from the central pre-main sequence star.

^b Ratio of the integrated FUV radiation field at 1 AU to the average interstellar radiation field ($1.6 \times 10^{-3} \text{ erg cm}^{-2} \text{ s}^{-1}$; Habing 1968).

^c Intrinsic $\text{Ly}\alpha$ emission, integrated over 1211 – 1221 Å.

^d Other stellar+accretion hot gas emission lines, C III $\lambda 977 \text{ \AA}$ + O VI $\lambda \lambda 1032, 1038 \text{ \AA}$ + N V $\lambda \lambda 1239, 1243 \text{ \AA}$ + He II $\lambda 1640 \text{ \AA}$.

^e Average quantities are calculated excluding DR Tau, whose $\text{Ly}\alpha$ profile reconstruction is compromised by multiple $\text{Ly}\alpha$ emission sources (§A.1).

●主に注目している点

- Flux of FUV radiation field: interstellar radiation field の 10^7 倍

- Total FUV emission: $\text{H}\alpha \sim 88\%$, FUV continuum $\sim 8\%$, 両方ともCIVとの相関あり

→accretion process がこれらの成分の生成に支配的??

- Lyman limit (912Å) と $\text{H}_2(0-0)$ absorption band (1100Å) 間のemissionは全体の $\sim 0.5\%$ のみ